Novel Approach to Tuning the Physical Properties of Organic-Inorganic Hybrid Semiconductors

Yong Zhang,[1,*] G. M. Dalpian,[1] B. Fluegel,[1] Su-Huai Wei,[1] A. Mascarenhas,[1] X.-Y. Huang,[2] J. Li,[2] and L.-W. Wang[3]

[1]*National Renewable Energy Laboratory, 1617 Cole Boulevard, Golden, Colorado 80401, USA*

[2]*Department of Chemistry, Rutgers University, Piscataway, New Jersey 08854, USA*

[3]*Computational Research Division, Lawrence Berkeley National Laboratory, Berkeley, California 94820, USA*

(Received 19 April 2005; published 20 January 2006)

We discuss theoretically a novel approach to tailoring the properties of a new family of organic-inorganic hybrid superlattices, using two isostructural materials, $ZnSe(en)_{0.5}$ and $ZnTe(en)_{0.5}$, as examples. Replacing Se with Te leads to a number of nontrivial changes: the conduction band parity, singularity type, conductivity in the superlattice direction, and the *p*-type dopability. Experimentally, we report the first unambiguous observation of exciton-polariton emission in a hybrid semiconductor, i.e., $ZnTe(en)_{0.5}$. The band-edge excitonic transitions in both emission and absorption are explained by the calculated electronic structures.

DOI: 10.1103/PhysRevLett.96.026405 PACS numbers: 71.35.−y, 71.36.+c, 73.21.Cd, 81.07.Pr

Organic-inorganic hybrid materials have attracted much attention in the past decade because of their tremendous potential in providing enhanced material properties that are not easily achievable with either organic or inorganic materials alone [1]. With a few exceptions [1], most hybrid materials do not have long-range order (typically with either amorphous organic or inorganic layers). Only recently has a new family of II-VI based fully ordered hybrid crystals been synthesized, and shown to exhibit unusual properties, such as a giant band gap tunability of 1–2 eV and a greatly enhanced band-edge excitonic absorption [2,3]. Among them are ultra-short-period organic-inorganic superlattices or quantum wells (3D or 2D structures) and single atomic bond quantum wire arrays (1D structures) [2].

The 3D structures, the first fully ordered and all-covalent chalcogenide hybrids [4], are particularly interesting. They are single II-VI semiconductor layers bridged by bidentate organic diamine molecules, which bear a close resemblance to the short-period inorganic superlattices (e.g., artificially grown GaAs/AlAs and spontaneously ordered InP/GaP superlattices) [5]. It has been generally believed that because organic materials have much larger band gaps (>5 eV) than inorganic materials, the organic molecules act as barriers and the hybrid materials possess the key electronic properties of a 2D system: the strong quantum confinement of both electrons and holes to the inorganic region, as confirmed in $ZnSe(en)_{0.5}$ [6], and the expected poor carrier conductivity in the superlattice direction.

Despite these general expectations, many important aspects of the materials have not yet been explored (for instance, the band alignment between the organic and inorganic materials and its effects on the electronic and optical transitions). These properties critically affect the transport and doping properties of the materials and their device applications. Furthermore, the most basic electronic and optical property of the materials (i.e., the band-edge excitonic optical transition, manifested in either absorption or emission) has not been clearly understood or measured. In this work, we focus on a specific hybrid system, $ZnTe(en)_{0.5}$ (en = ethylenediamine), and perform a combined experimental (i.e., spectroscopy) and theoretical (i.e., band structure calculation) investigation to address these issues. For the first time [7], free exciton-polariton emission at the fundamental band edge of a hybrid crystal is unambiguously observed at both low and room temperature (LT and RT) in $ZnTe(en)_{0.5}$. We find that, in striking contrast to its isostructures such as $ZnSe(en)_{0.5}$ [6], in $ZnTe(en)_{0.5}$, the electron at the conduction band minimum (CBM) is actually delocalized, despite that the second CBM remains localized in the inorganic region. Furthermore, unlike in $ZnSe(en)_{0.5}$, the Γ point free exciton emission in $ZnTe(en)_{0.5}$ is associated with a "parity-forbidden" interband transition [8] with a M_1 saddle point singularity [9,10], thus providing an unusual example of exciton-polaritons in solids.

The crystals of hybrid materials, α- and β-$A_{II}B_{VI}(en)_{0.5}$ [4] were grown under solvothermal conditions. Their structures were fully solved by single-crystal x-ray diffraction methods [2,4]. Although en, $C_2H_8N_2$, is an organic solvent at RT, it can form a molecular crystal at $T < 10\,^{\circ}\mathrm{C}$ [11]. The band gap of en is measured by absorption to be $E_g(\mathrm{en}) \approx 5.27 \pm 0.03$ eV at RT. The $A_{II}B_{VI}$ layer is a distorted $(1\bar{1}20)$ plane of the wurtzite or the (110) plane of the zinc-blende structure, respectively, for the α and β phase. The properties of the two phases are rather similar, except that the band gap of the α phase is larger typically by $\sim$0.2 eV. There are two nonequivalent $A_{II}B_{VI}$ layers in each period along the stacking direction. Unlike the bulk II-VI semiconductor, both α and β phases have inversion symmetry, where the inversion center is in the middle of the $(en)_{0.5}$ molecule layer. Raman studies on such crystals have shown very high crystallinity, with their Raman lines as sharp as those of any binary semiconductor [2].

Figure 1 shows the polarized photoluminescence (PL), absorption, and reflectance spectra of β-$ZnTe(en)_{0.5}$ mea-

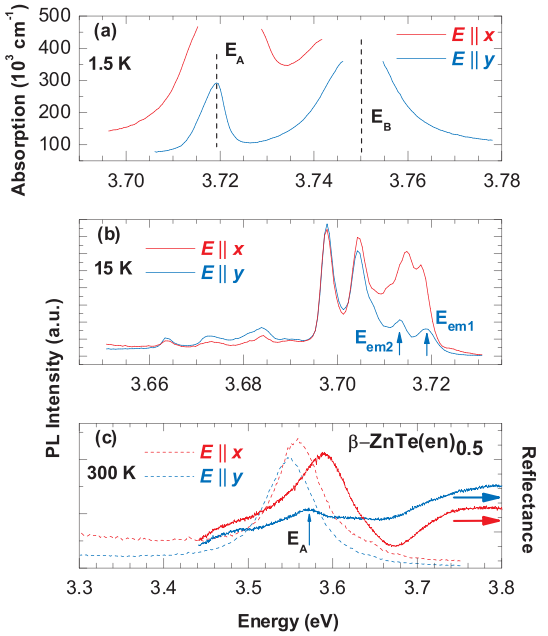

FIG. 1 (color). Polarized absorption, photoluminescence (PL), and reflectance spectra for β-ZnTe(en)$_{0.5}$. (a) Low temperature absorption, (b) low temperature PL, and (c) room temperature PL and reflectance.

sured at LT and RT. In these measurements, light is directed along the stacking direction of the superlattice z, with polarizations in either of the two in-plane principal axes x and y. As shown in Fig. 1(a), the excitonic peak is revealed only for the y polarization ($E \parallel y$) with a peak absorption of $\sim 3 \times 10^5$ cm^{-1} (a factor of 2 enhancement compared to $\sim 1.4 \times 10^5$ cm^{-1} for ZnTe[12]) [3], whereas for the x polarization ($E \parallel x$), the peak is too strong to reveal, but can be estimated to be $\sim 10^6$ cm^{-1}. The lowest free exciton absorption peak is at $E_A = 3.7192$ eV (a giant shift of 1.339 eV from that of 2.3805 eV for ZnTe[12]), with the second peak at $E_B = 3.7504$ eV (± 0.4 meV), and a splitting $\delta E_{AB} = 31$ meV. Two additional features were also observed in LT reflectance at $E_C = 3.870$ and $E_D = 3.890$ eV [3]. We notice that the $E \parallel y$ absorption profile appears to be asymmetrically broadened toward the lower energy side or quickly drops off on the higher energy side, in contrast to that of a typical M_0 exciton [e.g., ZnTe [12]], but resembling that of a M_1 exciton [9]. Shown in Figs. 1(b) and 1(c) are polarized PL spectra at LT and RT, respectively. In Fig. 1(b), with $E \parallel y$, an emission peak is observed at $E_{em1} = 3.7193$ eV $\pm$ 0.3 meV (with excitation density $\sim 5 \times 10^2$ W/cm^2 from the 325 nm laser line), which matches nicely with the absorption peak E_A. Strong anisotropy between $E \parallel x$ and $E \parallel y$ is observed for the emission near E_{em1}, and the line shape of $E \parallel x$ appears to be distorted by the strong absorption. Because the observed emission is polaritonic in nature, the emission peak in the vicinity of the absorption peak can be attributed to the upper polariton branch (UPB) and occurs at the vicinity of the longitudinal exciton energy (E_L). With $E \parallel y$, an additional peak at $E_{em2} = 3.7133$ eV or ~ 6 meV below might be attributed to the lower polariton branch (LPB) and is expected to be near the transverse exciton energy (E_T) [13]. Therefore, the longitudinal-transverse exciton splitting is tentatively determined as $\Delta E_{L\text{-}T} \approx 6$ meV, which is much larger than that of 0.6 meV for ZnTe [14]. Polarized PL provides an estimate for the $E \parallel x$ free exciton absorption that was too strong to obtain from direct absorption. The PL polarization ratio at the vicinity of E_A is ~ 3.7, which yields an estimated peak absorption $\sim 1.1 \times 10^6$ cm^{-1} for $E \parallel x$. The origins of a series of peaks within 21 meV below E_{em1} are of great interest. One would be tempted to speculate that they are related to shallow impurities. If so, they should have very different temperature and excitation density dependences from the free exciton transition at E_{em1}. But, we find that these peaks actually exhibit similar temperature and excitation density dependence to the E_{em1} peak, suggesting them to be rather the first-order LO phonon sidebands (PS's) of the free exciton emission (together with likely higher order features at lower energies) [15]. Indeed, a number of phonon modes have been observed in that frequency region [2]. At $T >$ 100 K, the zero-phonon line E_{em1} becomes unresovable and convoluted together with all the PS's into one broad band. Figure 1(c) shows the PL and reflectance spectra at RT, where the free exciton emission band at 3.548 eV exhibits a Stokes' shift from the band gap at 3.571 eV (for $E \parallel y$) due to the PS contribution.

To gain more insight into the electronic properties of the hybrid materials, we perform band structure calculations for α or β-ZnTe(en)$_{0.5}$ (αZT or βZT, thereafter) and compared them with α-ZnSe(en)$_{0.5}$ (αZS), with the structures determined by x ray [2,4], using a first-principles plane-wave pseudopotential method within the local density approximation (LDA). The pseudopotentials are generated with $3d$ electrons of Zn treated as valence electrons, and with core corrections for Te and Se. A 70 Ry energy cutoff is used. Spin-orbit interactions are included in the calculations. In addition, a full-potential linearized augmented plane-wave (FLAPW) and a projector augmented wave (PAW) method, also within the LDA, are used for calculating band alignments and dielectric constants. Our calculated band gap shifts, $E_g(\beta\text{ZT}) - E_g(\text{ZnTe}) = 1.381$ eV, $E_g(\alpha\text{ZT} - E_g(\text{ZnTe}) = 1.668$ eV), and $E_g(\alpha\text{ZS}) - E_g(\text{ZnSe}) = 1.435$ eV, are in good agreement with experimental results [2].

Because of the existence of two inorganic slabs in each period, the electronic states near the band edge always appear in pairs, and the splitting between the two complementary states reflects the coupling between the two slabs. The separation of the first pair of conduction bands (CB1 and CB2) at the Brillouin-zone (BZ) center Γ point (CB1Γ and CB2Γ) are $\delta E_{CB} = 82$ meV, 140 meV, and 242 meV,

respectively, for αZT, βZT, and αZS; the separation of the first pair of valence bands (VB1 and VB2) at the Γ point (VB1Γ and VB2Γ) are $\delta E_{\mathrm{VB}} = 20.3$ meV, 20.4 meV, and 28.4 meV, respectively. These one-electron energies provide a reasonable account for the optical transitions involving excitonic states in βZT: δE_{AB} and δE_{CD} are due to the VB splitting δE_{VB}, and $\delta E_{\mathrm{AC}} \approx 150$ meV is due to the CB splitting δE_{CB}. Note that the excitonic effect, to be discussed later, will induce a coupling between the split bands, and thus alter the splitting.

It has been shown that for αZS, the wave functions of the CB1Γ and VB1Γ are both strongly localized in the ZnSe layers [6], as one may expect based on the large band gap difference between en and ZnSe. Surprisingly, we find that αZT or βZT is very different from αZS: (1) the CB1Γ wave function is not localized in the ZnTe slab, but distributed throughout the whole structure. (2) In αZT or βZT, the CB1Γ has even parity and CB2Γ has odd parity, opposite to the parity order in αZS. Figure 2 shows the comparison between αZT and αZS for their CB wave functions. Because the VB1Γ is always more localized in the II-VI layers and has even parity for all three structures, the interband dipole transition is thus allowed between VB1Γ and CB1Γ in αZS, but forbidden in αZT or βZT. If it were a typical Wannier exciton case, one would consider the band-edge excitonic transition to be parity (dipole) forbidden in αZT or βZT. However, the excitonic absorption is actually exceedingly strong, as shown in Fig. 1(a) for βZT, compared to a textbook example of the parity-forbidden excitonic transition in Cu_2O, where the 1s absorption strength is merely 3 cm^{-1} [8,16]. (3) For αZS, both the CB1 and the VB1 are found to have positive effective masses in all three principal directions [6]; thus, the Γ point has a M_0 singularity in the joint density of states (JDS's). In contrast, in αZT or βZT, the CB1 has a negative effective mass m_z in the z direction, which results in a M_1 singularity or saddle point in the JDS's. This is in contrast to conventional semiconductors (IV, III-V, and II-VI), which typically show a saddle point at critical points away from the BZ center (e.g., the L point) [9,10]. The effective masses are listed in Table I for βZT.

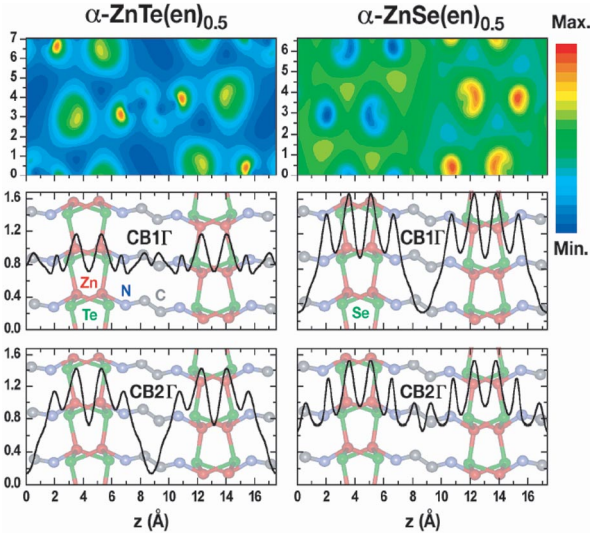

FIG. 2 (color). Conduction band wave functions of α-ZnTe(en)$_{0.5}$ (left column) and α-ZnSe(en)$_{0.5}$ (right column): the first row gives the real part wave function of CB1Γ on an x-z plane centered at the unit cell; the second and third row, respectively, show the charge densities (the wave function squares) of CB1Γ and CB2Γ, integrated over the x-y planes. β-ZnTe(en)$_{0.5}$ is qualitatively similar to α-ZnTe(en)$_{0.5}$. The structure of each material is shown in the background of the figures as a guide to the eye.

We find that all these intriguing features of αZT and βZT can be understood by examining the band alignments among en and the ZnSe and ZnTe layers. Figure 3 presents our calculated band offsets between βZT, ZnTe, ZnSe, and en using the FLAPW method and a core-level aligning procedure [17]. Despite that E_g(ZnTe) is $\sim$0.4 eV smaller than that of E_g(ZnSe) [18], the CBM of ZnTe is $\sim$0.3 eV above that of ZnSe [17], because the Te 5s orbital energy is significantly higher than the Se 4s orbital. It is the higher CBM of ZnTe that is responsible for the three nontrivial consequences mentioned above. In fact, by artificially lowering the s component of the Te pseudopotential, one can induce a switch of parities between CB1Γ and CB2Γ and a change of the critical point type from M_1 to M_0. Note that for the primarily s-derived CB1Γ and CB2Γ in all three structures studied here, independent of their energy order, the odd parity (antisymmetric) state always has higher charge distribution in the inorganic region than the even (symmetric) state. Thus, one should expect that lowering the electron potential in the inorganic region, which results in more energy lowering for the antisymmetric than the symmetric state, may lead to the parity switch between the CB1Γ and CB2Γ. It is particularly interesting to note that in αZT and βZT, despite the CB1Γ state being significantly below the barrier, as shown in Fig. 2, its wave function is actually delocalized along the z direction, and counterintuitively, the higher CB2Γ state is much more localized than the CB1Γ state in the inorganic region. This observation is practically important, because electrons at the CBM could have good conductivity along the z direction in αZT and βZT, but not in αZS. Figure 3 also indicates that the ultrathin inorganic slab has already yielded a significant amount of blueshift in band gap compared to the bulk semiconductor. These analyses in-

TABLE I. Effective masses for the first and second conduction and valence band in three principal directions for β-ZnTe(en)$_{0.5}$.

	x	y	z
CB1	0.287	0.353	−4.274
CB2	0.165	0.294	−0.463
VB1	0.585	0.861	10.310
VB2	0.0966	1.029	−9.990

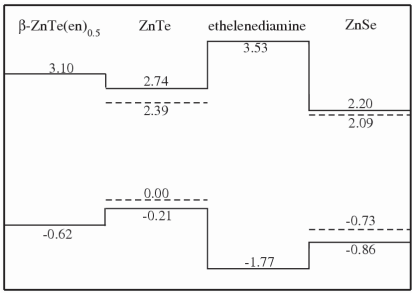

FIG. 3. Energy alignments of the conduction and valence band edges for ZnTe, ZnSe, ethylenediamine, and β-ZnTe(en)$_{0.5}$. The dashed and solid lines in the inorganic sections are, respectively, for the bulk and isolated slab. The conduction band energies have been adjusted from the LDA values to the appropriate experimental values.

dicate that due to the ultrathin and double quantum well nature of the hybrids, the electronic properties of these hybrid materials cannot simply be described by quantum confinement effect, as one might intuitively think [4,6]. These understandings provide the insights to manipulate the electrical and optical properties of the hybrid materials. For example, to improve electron conductivity along the superlattice direction, our analyses suggest that we should choose materials such as ZnTe(en)$_{0.5}$ that have a relatively high CBM. Furthermore, according to an empirical doping pinning rule [19], ZnTe(en)$_{0.5}$ with a relatively high valence band maximum should also have good p-type dopability, in contrast to other large-band-gap semiconductors (e.g., ZnO and GaN) with a p-type doping difficulty.

Finally, we discuss the excitonic effect in βZT. For a M_1 saddle point with strong anisotropy [9], as in the case of βZT, the absorption peak is expected to appear at an energy close to $E_g - E_b^{2D}$, where E_b^{2D} is the corresponding 2D exciton binding energy. The high frequency dielectric constants have been calculated using PAW: $\varepsilon_x = 6.06$, $\varepsilon_y = 5.41$, and $\varepsilon_z = 4.88$, compared to $\varepsilon_\infty = 7.28$ for ZnTe [18]. The exciton binding energy can be estimated using a 2D variational model: $E_{\mathrm{exA}}^{2D} = 427$ meV for CB1/VB1 and $E_{\mathrm{exB}}^{2D} = 259$ meV for CB1/VB2. The binding energy is only 13 meV in ZnTe [20]. A strong coupling between the two excitonic bands is expected based on the fact that $E_{\mathrm{ex}}^{2D} \gg \delta E_{\mathrm{VB}}$. The large binding energy in the hybrid indicates that the exciton wave function, thus the intensity and polarization of the free excitonic optical transition, should include the contributions from a large region of the **k** space in the BZ [21]. We find that although the dipole matrix element is zero at Γ, it increases rapidly when moving away from Γ, and is much larger for the x polarization, which provides a qualitative explanation for the experimentally observed strong absorption and anisotropy near the band edge. The relaxation of the parity selection rule observed in systems such as βZT is distinctly different from that in Cu_2O. For the latter, it is due to the quadrupole transition, which remains weak. For the former, it is due to the extended spread of exciton wave function in **k** space, where the normal parity selection rule becomes practically irrelevant.

In summary, we have shown that the physical properties of the hybrid can be tuned drastically by using different inorganic components with different band alignments. This study provides important hints on how to tailor the material properties by properly selecting the inorganic and organic component in a hybrid structure or even by alloying two hybrids with different inorganic components.

We thank H. X. Fu for valuable discussions and J. Pern for assistance in the absorption measurement of en. The work at NREL was supported by DOE and NREL DDRD, at Rutgers by NSF (DMR-0422932), and at LBNL by DOE. The computing resources were provided by NERSC at LBNL and CSC at NREL.

*Email address: yong_zhang@nrel.gov

[1] D. B. Mitzi, in *Progress in Inorganic Chemistry*, edited by Karlin (Wiley, New York, 1999), p. 1; T. Ishihara, in *Optical Properties of Low-Dimensional Materials*, edited by T. Ogawa and Y. Kanemitsu (World Scientific, Singapore, 1995), p. 289.
[2] X. Y. Huang *et al.*, J. Am. Chem. Soc. **125**, 7049 (2003).
[3] B. Fluegel *et al.*, Phys. Rev. B **70**, 205308 (2004).
[4] X. Y. Huang *et al.*, J. Am. Chem. Soc. **122**, 8789 (2000).
[5] J. H. Li *et al.*, Phys. Rev. Lett. **91**, 106103 (2003); A. Mascarenhas, *Spontaneous Ordering in Semiconductor Alloys* (Kluwer Academic/Plenum Publishers, New York, 2002).
[6] H. X. Fu and J. Li, J. Chem. Phys. **120**, 6721 (2004).
[7] X. Hong *et al.*, Phys. Rev. B **45**, 6961 (1992); an emission within 10 meV from the excitonic absorption peak is attributed to the free exciton recombination.
[8] R. J. Elliott, Phys. Rev. **124**, 340 (1961).
[9] E. O. Kane, Phys. Rev. **180**, 852 (1969).
[10] M. Cardona and G. Harbeke, J. Appl. Phys. **34**, 813 (1963).
[11] V. R. Thalladi *et al.*, Angew. Chem., Int. Ed. **39**, 918 (2000).
[12] H. Leiderer *et al.*, Semicond. Sci. Technol. **6**, A101 (1991).
[13] E. Gross *et al.*, Solid State Commun. **10**, 1071 (1972); D. D. Sell *et al.*, Phys. Rev. B **7**, 4568 (1973).
[14] H. Venghaus *et al.*, Solid State Commun. **33**, 371 (1980).
[15] H. Sumi, J. Phys. Soc. Jpn. **41**, 526 (1976).
[16] E. F. Gross and A. A. Kaplyanskii, Dokl. Akad. Nauk SSSR **139**, 75 (1961) [Sov. Phys. Dokl. **6**, 592 (1962)].
[17] S.-H. Wei and A. Zunger, Appl. Phys. Lett. **72**, 2011 (1998).
[18] O. Madelung, *Semiconductors—Basic Data* (Springer, New York, 1996).
[19] S. B. Zhang *et al.*, J. Appl. Phys. **83**, 3192 (1998).
[20] H. Venghaus and P. J. Dean, Phys. Rev. B **21**, 1596 (1980).
[21] G. M. Kavoulakis *et al.*, Phys. Rev. B **55**, 7593 (1997).